Antibacterial Activity of Mesoporous Silica Nanofibers

Sohrabnezhad, Shabnam**+; Jafarzadeh, Abolfazl

Department of Chemistry, Faculty of Science, University of Guilan, Rasht, I.R. IRAN

Rassa, Mehdi

Department of Biology, Faculty of Science, University of Guilan, Rasht, I.R. IRAN

ABSTRACT: *In this research, the fabrication of MCM-41 mesoporous material nanofibers by an electrospinning technique was performed. The MCM-41 nanofibers (MCM-41 NFs) as a novel host on the incorporation of silver has been studied in $[Ag(NH_3)_2]NO_3$ precursor solution through the heat-treatment process. The formation of silver-loaded MCM-41 NFs at various calcinating temperatures were also studied. The silver-containing materials (Ag/MCM-41 NFs) were characterized using Fourier Transform InfraRed (FT-IR) spectroscopy, powder X-Ray Diffraction (XRD), Scanning Electron Microscopy (SEM), UltraViolet-Visible Diffuse Reflectance Spectroscopy (UV-Vis DRS), and Transmission Electron Microscopy (TEM). The results indicated that both Ag and Ag_2O NanoParticles (NPs) were loaded in MCM-41 NFs at different calcinating temperature. Silver compounds with a diameter of 10−15 nm were highly dispersed in the framework of mesoporous silica nanofibers. The results indicated that Ag loading contents on the MCM-41NFs were 10.53 wt%. These Ag/MCM-41 NFs Possess an enhanced antibacterial effective against both Gram-positive and Gram-negative bacteria by preventing the aggregation of silver NPs and continuously releasing silver ions. In general, the silver-containing materials with more Ag_2O NPs demonstrated an excellent antibacterial activity. The Minimum Inhibitory Concentrations (MIC) obtained 30 and 60 µg/mL for the silver-containing MCM-41 NFs with more Ag_2O NPs against E. coli and S. aureus, respectively. MCM-41 type nanofibers play an important role in the antibacterial activity of nanocomposites.*

KEYWORDS: *MCM-41 nanofibers; Ag/MCM-41 nanofibers; Antibacterial activity; Ag_2O-MCM-41 nanofibers; Diffuse reflectance spectroscopy*.

INTRODUCTION

Metallic silver or its ions have long been known to have strong inhibitory and antibacterial effects as well as a broad spectrum of antibacterial activities. Therefore, silver has been commercially used to take advantage of its antibacterial properties [1]. However, such free NPs are an unsuitable presentation format for medical devices, topical application and prolonged silver release are needed. Anchoring on a suitable matrix reduces or eliminates the environmental risk of the NPs and improves their stability. The antibacterial activity of simple or composite Ag NPs has been reported in several recent studies [2–6], in which the oxidation of Ag NPs limits their practical

** To whom correspondence should be addressed.*
+ E-mail: sohrabnezhad@guilan.ac.ir
1021-9986/2020/3/1-11 11/$/6.01

application, as aggregation may cause degradation or even loss of their antibacterial activity [7]. The use of mesoporous materials as an Ag carrier to overcome this problem has attracted wide attention. For antibacterial applications, Ag-mesoporous materials offer many advantages, such as (1) higher stability of the Ag ions in the porous matrix (the dispersion of Ag ions within a porous structure prevents their agglomeration and oxidation in the air) [8, 9] and (2) the long-term antibacterial activity of nanocomposites because of the controlled release of Ag ions from the porous matrix [10]. The synthesis of Ag-containing mesoporous materials has widely been reported as matrices for adsorption of silver ions or nanoparticles [10-12], due to their large specific surface area, regular pore structure, and highly controllable surface properties [13]. However, most studies on mesoporous silica materials have focused on materials synthesized in bulk or powder form. On the other hand, silver-supported silica materials, such as silica glass [14] and silica thin films [15], indicated to be good candidates' antibacterial materials due to their fine chemical durability and high antibacterial activity. However, to the best of our knowledge, no study has examined the synthesis of MCM-41 mesoporous nanofibers containing Ag NPs or Ag-compounds in antibacterial applications.

Pure siliceous MCM-41 material possesses many unique properties such as high surface area, high pore volume, as well as parallel and ideally shaped pore structures without the complications of a network [16]. There are several papers about the synthesis of mesoporous fibers by different methods such as sol-gel process [17], spray-drying method [18], laser deposition [19], solvent evaporation techniques [20], and emulsion methods [17]. But these methods had complex processes and sometimes the length of fibers is limited by the fibrous template. Therefore a practicable and simple method is needed to prepare ultrafine and long molecular sieve fibers for adsorption of NPs and pollutant compounds. Electrospinning is the most simple and flexible way to fabricate continuous fibers in micro and nanoscale. In the electrospinning process, a viscous solution is pumped to a high electric field [21].

In this work, we report for the first time synthesis of MCM-41 mesoporous material nanofibers from the solution containing of polyvinyl alcohol (PVA) as the polymeric gelator, cetyltrimethylammonium bromide (CTAB) as the template source and tetraethyl orthosilicate (TEOS) as the silica source, by electrospinning technique in acidic media. MCM-41 NFs were then used as a novel matrix for the incorporation of silver compounds (Ag and Ag_2O NPs). By TEM, XRD, SEM and DRS, it was found that more Ag could be loaded on the MCM-41 NFs when $[Ag(NH_3)_2]NO_3$ was used as Ag precursor, as compared to $AgNO_3$ as the precursor. The main aim of this study was to investigate the effect of nanofibers morphology on the loading of silver and its antibacterial activity against Gram-negative *Escherichia coli* (*E. coli*), Gram-positive *Staphylococcus aureus* (*S. aureus*).

EXPERIMENTAL SECTION

Materials

All chemicals (tetraethyl orthosilicate (TEOS), cetyltrimethylammonium bromide (CTAB), hydrochloric acid, polyvinyl alcohol (PVA, M_W ~ 72000), absolute ethanol, and sodium hydroxide), ammonia (25 W%), and $AgNO_3$ were analytical grade. Deionized water was used throughout this work.

Synthesis of MCM-41 NFs

Cetyltrimethylammonium bromide (CTAB, 0.43 g) was added into 1.93 g absolute ethanol under stirring. After stirring for 20 min, 2.08 g TEOS and then 0.41 ml HCl 0.12 M was slowly added to the resulting mixture. The molar ratio of the composition was TEOS: 0.12 CTAB: 0.005 HCl: 4.2 EtOH: $7H_2O$: 0.1PVA (repeat unit). The reaction mixture was transferred in a glass vial. The closed vial was placed in an oven at 80°C for 2 h, and thereafter left open at 25°C for two days (low temperature promotes condensation between silica oligomers and increases calcination stability of the mesostructured phase). After two days a 4 wt% aqueous solution of polyvinyl alcohol (PVA, M_W ~ 72000) was added to the mixture under vigorous stirring until a clear, homogeneous, viscous, and spinnable solution was obtained and used as the feeding solution for electrospinning.

Electrospinning procedure and removal compound

The electrospinning was set up horizontally. The spinnable feeding sol was poured into the plastic syringe

equipped with a gauge needle made of stainless steel, which was connected to a high-voltage DC supplier. During the electrospinning process, the feeding sol was pressurized by tracing injection device. The driven voltage applied was in 12 kV, and the distance between the needle and the flat aluminum foil collector was 10 cm and finally, the electrospinning process was conducted under ambient temperature, and then nanofibers were air-dried at 110°C for 10 h. The extraction of the template was carried out using the mixture of 1 g of electrospun MCM-41 and 100 ml of acidified ethanol (1 mol of concentrated HCl: 10 mol of ethanol) under magnetic stirring at ambient room temperature for 24 h (only for electrospun MCM-41 from amorphous silica). After that, the samples were calcined at 600°C at a rate of 3°C/min for 3 h. All electrospun samples were white color after calcination. During calcination, mesoporous material undergoes further condensation, CTAB, and polymer are removed. With temperature and calcination, the nanofibers become brittle.

Synthesis of Ag_2O NPs

The Ag_2O NPs were synthesized through a wet chemical technique. 80 mL of a 0.005 M silver nitrate aqueous solution was heated to 60ºC. After that 20 mL of a 0.025 M sodium hydroxide aqueous solution was added drop-wise, while the solution was constantly stirred with a magnetic stir bar, until the solution had the consistency of a gray-yellow colloidal suspension. The reaction of silver nitrate with sodium hydroxide produces silver hydroxide via the following mechanism:

$$AgNO_3 + NaOH \longrightarrow AgOH + Na^+ + NO_3^-$$

The intermediate AgOH is thermodynamically unstable, and ultimately produces Ag_2O through the following recombination process:

$$2AgOH \longrightarrow Ag_2O + H_2O \ (pK = 2.875)$$

The solution was kept at 60ºC for 2 h to ensure complete reaction. The particles were then collected in 3 cycles of a centrifuge/re-dispersion washing process using ethanol, and the solution was allowed to dry, leaving behind the brown Ag_2O particles.

Synthesis of silver containing MCM-41 NFs (Ag/MCM-41 NFs)

To increase the silanol groups on the surface of MCM-41 NFs, the calcined MCM-41 NFs was rehydroxylated by 0.1 M hydrochloric acid for 1 h. After washing and drying of nanofibers, 1.0 g of the MCM-41 NFs was immersed in 150 ml of biamminesilver nitrate ($[Ag(NH_3)_2]NO_3$) solutions, which were formed by adding 25 wt% aqueous ammonia into $AgNO_3$ solution at room temperature and pH 9.0 adjusted with HNO_3 solution in brown bottles. The concentration of biamminesilver nitrate was 0.1 M. After soaking for 12 h, the NPs were separated and washed with deionized water, then dried in vacuum at 40 ºC for 4 h. Finally, the nanocomposites were calcinated in the air at 500 and 600 ºC for 3 h to decompose $[Ag(NH_3)_2]$+ ions and yield Ag NPs on the nanofibers. The prepared nanocomposites were termed as 500Ag/MCM-41NFs and 600Ag/MCM-41NFs, respectively.

Green Synthesis of Ag nanoparticles

A 10 g of *Urtica dioica* leaves was stirred with 100 mL de-ionized water at 60◦C for 24 h, and filtered to get the extract. The filtrate is used as a reducing agent and stabilizer. 1.0 mL of leaf extract was added to 2.0 mL of 1.0×10^{-2} M $AgNO_3$ and the volume was adjusted to 10 mL with double distilled water for the green reduction process. After about 15 min, the nanoparticles were separated and washed with deionized water, then dried in vacuum at 40 ºC for 4 h [4].

Characterization

Powder X-ray diffraction patterns of the samples were recorded using an X-ray diffractometer (Bruker D8 Advance) with Co Kα radiation (λ = 1.789 A˚) under the conditions of 40 kV and 30 mA, at a step size of 2Θ = 0.02˚. X-Ray Diffraction (XRD) patterns were recorded between 2˚ and 70˚ 2Θ at a scanning speed of 2˚/min. All samples were analyzed in random orientation. The UV–Vis diffused reflectance spectra (UV–Vis DRS) were obtained with a UV–Vis Scinco 4100 spectrometer with an integrating sphere reflectance accessory. $BaSO_4$ was used as a reference material. UV–Vis absorption spectra were recorded using a Shimadzu 1600 PC in the spectral range of 190-900 nm. The infrared spectra were measured on a Bruek spectrophotometer using KBr pellets. For each sample, 128 scans in the 4000-400 cm^{-1} spectral range were recorded with a resolution of 2 cm^{-1}. Samples of 0.5 mg were dispersed in 200 mg of KBr.

The Transmission Electron Micrographs (TEM) were recorded with a Zeiss-EM10C microscope, working at 80 kV accelerating voltage. Samples for TEM were prepared by dispersing the powdered sample in acetone by sonication and then drip dry on a copper grid coated with carbon film. Samples were sonicated for 15 minutes. Chemical analysis of the samples was done by Energy Dispersive X-ray (EDX) analysis joined to a Philips XL 30 scanning electron microscopes. The surface morphology of the samples was obtained using a Jeol-JSM-5610 LV scanning electron microscopy (SEM).

Evaluation of antibacterial properties

Antibacterial studies were carried out using *Escherichia coli (E. coli*) and *Staphylococcus aureus* (*S. aureus*) culture. The reagents, media, and solutions were prepared with distilled water and analytical grade reagents. The glassware and accessories used in this study were washed and sterilized in an autoclave at 121˚C for 15 min. Determination of the minimum inhibitory concentrations (MIC) of the 500Ag/MCM-41NFs and 600Ag/MCM-41NFs nanocomposites was carried out using a nutrient broth solution of 8 g/L. This nutrient broth solution was added to tubes such that the final concentrations of the nanocomposites were 15-1000 µg/mL. The bacterial culture was grown to log phase and added to the tubes containing the sample solutions to obtain a count of ~10^8 colony-forming units (cfu/mL). The tubes were incubated at 37 ˚C for 24 h. At the end of the incubation period, the minimum inhibitory concentration was determined by checking for the tube that did not show any visible growth. The MIC concentration and higher concentration were cultivated on nutrient agar for determining the Minimum Bactericidal Concentration (MBC).

RESULTS AND DISCUSSION

Structure analysis of samples

The powder X-ray diffraction patterns of the electrospun MCM-41 are shown in Fig. 1. The dried MCM-41 NFs showed diffraction peaks at 2θ = 2.26° (100), 3.92° (110), 4.53° (200), and 5.95° (210) that corresponds to a hexagonal structure from MCM-41 (Fig. 1a). Although only the three diffraction peaks were observed for the calcined MCM-41 nanofibers at 2θ = 2.45°, 4.28° and 4.95° (Fig. 1b). These hexagonal structures were attributed to MCM-41 mesoporous material [22]. The increase in peak intensity after calcination was due to the greater scattering density contrast and reduced X-ray absorbance after surfactant and polymer removal. Furthermore, the d-value related to (100) reflection decreased from 39 to 36 A° on calcination, corresponding to a moderate contraction in the mesoporous structure. In the synthesis of MCM-41 NFs, the mixture was in an acidic alcohol/water medium. During spinning, all solvents (alcohol and H_2O) were evaporated and the nonvolatile components (TEOS, PVA, and CTAB) self-assembly produces the hexagonally ordered MCM-41 mesophase structure.

To study the effect of the calcinating temperatures on the incorporation of silver on the MCM-41NFs, nanofibers after soaking in $[Ag(NH_3)_2]NO_3$ solution was treated in the air for 3 h at 500 and 600 ◦C, respectively. Fig. 2 shows the XRD patterns of the samples calcinated at different temperatures. It demonstrated that no obvious silver diffraction peaks were detected after the sample was calcinated at 500°C, except diffraction peak at 2θ values of 26.5°, 32.7°, 45.6°, and 55.21° can be indexed to (110), (111), (220), and (220) crystal planes of the Ag_2O phase (JCPDS No. 75-1532) [23]. As the heating temperature rose (600°C), peak intensity related to Ag_2O decreased, but more diffraction peaks of silver nanoparticles appeared and became remarkable at 2θ values of 38.2◦, 44.3◦, and 64.5◦ respectively, corresponding to the (111), (200), and (220) planes of silver (JCPDS No. 65-2871) [24]. Silver diffraction peaks are probably the results of the decomposition of the thermolabile Ag_2O, which breaks into Ag and O_2 at temperatures over 500ºC [25]. Two peaks at 2θ values of 2.5°and 4.53°corresponding to the diffraction planes (100) and (200), respectively, indicated that the MCM-4NFs catalyst included the typical highly ordered hexagonally mesoporous structure and the silver-containing MCM-41NFs maintained the structure of MCM-41NFs.

UV-Vis diffuse reflectance spectra analysis

UV-Vis diffuse reflectance spectra of the nanocomposites may reflect their ability to antibacterial activity, based on the type of silver compound synthesized in MCM-41NFs. The UV-Vis DRS of the different samples are shown in Fig. 3. The MCM-41NFs matrix no-showed

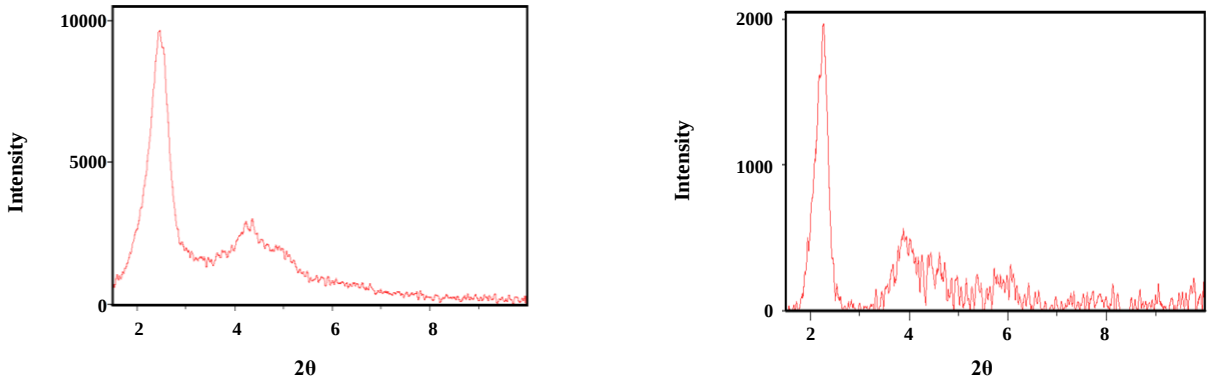

Fig. 1: XRD patterns of electrospun MCM-41 nanofibers (a) before (b) after calcination. Spinning voltage 12 kV and distance 10 cm.

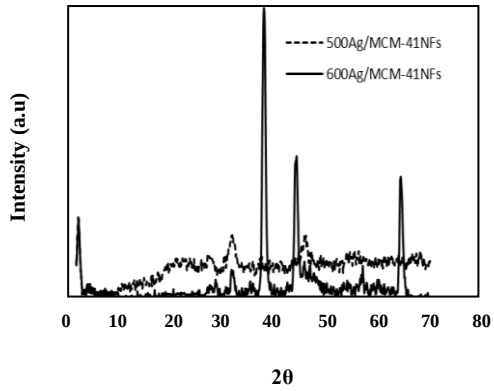

Fig. 2: XRD patterns of silver containing MCM-41NFs samples calcinated at different temperatures.

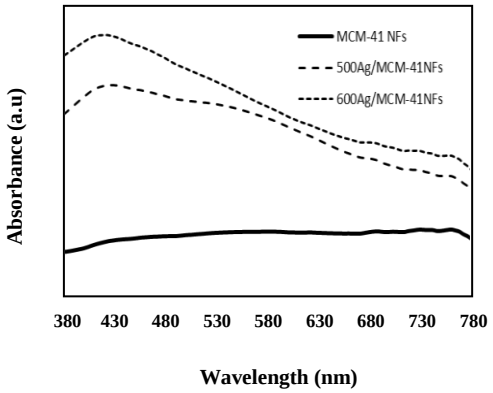

Fig. 3: Diffuse reflectance spectra of the samples.

peaks at 380 to 780 nm, which was similar to the other article [26]. The UV-Vis spectra of 500Ag/MCM-41NFs sample exhibit a wide visible light absorption band around 400-600 nm that assignable to the Ag_2O NPs [27]. As shown in Fig. 3, the 600Ag/MCM-41NFs nanocomposite indicated, an absorption band at 415 nm, which was attributed to the Localized Surface Plasmon Response (LSPR) of the Ag NPs [28]. With respect to 500Ag/MCM-41NFs nanocomposite, 600Ag/MCM-41NFs nanocomposite showed stronger absorption at 415 nm.

SEM and TEM images study

The morphology and microstructure of MCM-41NFs and Ag/MCM-41NFs nanocomposites were investigated by SEM observation. The electrospun MCM-41NFs (Fig. 4a) showed a smooth surface with an average diameter of 200-300 nm before and after the coating of Ag compounds and lengths of up to hundreds of micrometer. Fig. 4b showed SEM image of the Ag/MCM-41NFs calcinated at 500°C, which possesses rough surface owing to the presence of Ag_2O NPs over nanofibers and was similar to the other literature [27]. When the Ag/MCM-41NFs were calcinated at 600°C, SEM image (Fig. 4c) indicated a smooth surface for MCM-41 NFs again. The smooth surface of 600Ag/MCM-41NFs after calcination revealed that the Ag_2O NPs over matrix were broken into Ag and O_2 at temperatures over 500ºC.

TEM images (Fig. 5) of the samples confirmed the formation of a spherical Ag_2O and Ag NPs on the surface of 500Ag/MCM-41NFs and 600Ag/MCM-41NFs nanocomposites. It was observed that the Ag_2O and Ag NPs have uniformly distributed the surface of the MCM-41NFs without aggregation, with diameters in the range of 10–15 nm.

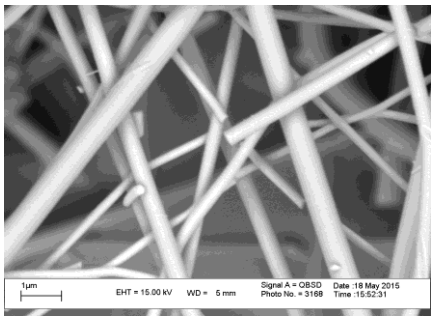

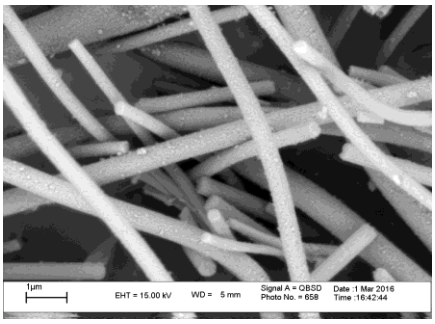

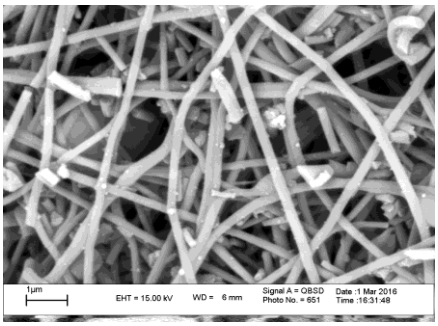

Fig. 4: SEM images of (a) MCM-41nanofibers, (b) 500Ag/ MCM-41NFs and (c) 600Ag/MCM-41 NFs samples.

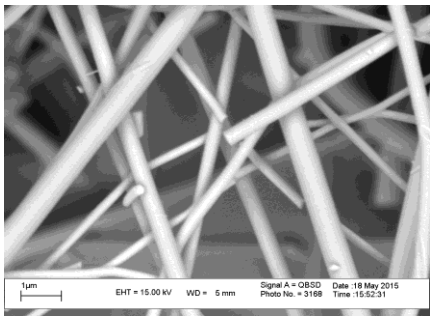

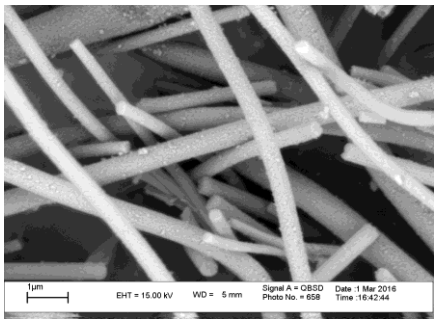

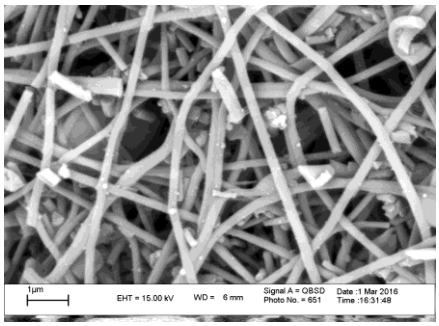

Fig. 5: TEM images of the samples.

Determination of Ag loading contents and released silver from samples

Atomic Absorption Spectroscopy (AAS, SpectraA 110, Varian) was used to quantify the amount of silver released to the media studied. A hollow cathode silver detection lamp (338 nm wavelength) and an air/acetylene burner were used for the determination. Atomic absorption standard solutions were prepared by diluting silver atomic absorption standard solution 1.0 wt.% HNO_3 (Sigma Aldrich) at the appropriated concentrations and used for the calibration of the equipment. Three independent measurements are automatically averaged for each sample. For the analytical determination of silver in culture media, 10 mL of culture media (without bacteria) was added under sterile conditions to plastic tubes containing (3.0-0.3) mg of each material (Table 1).

Table 1: The loading contents of Ag in MCM-41NFs and amount of silver released from samples obtained with AAS.

samples	Con. Of Ag precursors (M)	M (mg)	C_{Ag+} (μg/mL)	W_{Ag} (%)
500Ag/MCM-41NFs	0.1	3	1.5	10.53
600Ag/MCM-41NFs	0.1	3	0.9	10.53
Ag NPs	0.1	0.3	0.0 7	-
Ag_2O NPs	0.1	0.3	0.13	-

These solutions were sterilized and diluted with sterile deionized water. Dispersions were subsequently incubated at 37 °C for 24 h in the dark in an orbital incubator at 150 rpm. After the corresponding time, tubes were centrifuged at 10,000 rpm during 10 min and the collected supernatants were analyzed using AAS. Table 1 showed released silver from samples.

The loading amount of Ag in the MCM-41NFs matrix could be determined by dissolving a certain amount of Ag-supported MCM-41NFs (0.04 g) into 6 mL aqueous solution of $AgNO_3$ (0.1 M). After 24 h, suspensions were centrifuged and collected supernatants were analyzed using AAS. The results indicated that Ag loading content on the MCM-41NFs was 10.53 wt%.

The antibacterial property of synthesized materials

Silver is well-known for its strong inhibitory and antibacterial effects [29]. Synthesized nanocomposite materials, 500Ag/MCM-41NFs and 600Ag/MCM-41, were investigated to determine their antibacterial properties against *E. coli* and *S. aureus* bacteria and their results were shown in Table 2. 500Ag/MCM-41 NFs (Ag content is 3.15 μg/mL) at a concentration of 30 μg/mL can significantly inhibit the growth of E. coli in 24 h and before the bacteria starts to grow (MIC). When the concentration of 500Ag/MCM-41 NFs reached 60 μg/mL (Ag content is 6.31 μg/mL), the growth of *E. coli* can be completely inhibited (99.99% of *E. coli* was killed (MBC)). As *S. aureus* has a thicker cell wall than Gram-negative bacteria *E. coli*, it requires a higher Ag dose to inhibit the growth of *S. aureus* [30]. In our experiment, the growth of *S. aureus* significantly decreased when the concentration of 500Ag/MCM-41 NFs reached 60 μg/mL (Ag content was 6.31 μg/mL). When the concentration of 500Ag/MCM-41 NFs increased to 120 μg/mL (Ag content was 12.63 μg/mL), the growth of *S. aureus* can be completely inhibited (99.99% of *S. aureus* is killed in the first time). The MIC and MBC concentration were obtained 120 μg/mL (Ag content was 12.62 μg/mL) for 600Ag/MCM-41NFs sample against *E. coli*, and they were found 120 (Ag content was 12.62 μg/mL) and 250 μg/mL (Ag content was 26.32 μg/mL) against *S.aureus*, respectively (Table 2). In our study, the effective concentration of Ag/MCM-41nanocomposites was lower than that of previously reported Ag−Si nanocomposites [10, 12, 31, 32]. The Ag/MCM-41 NFs nanocomposites exhibit an excellent antibacterial activity in Gram-negative bacteria *E. coli* and Gram-positive bacteria *S. aureus*. To further show the advantages of Ag/MCM-41 NFs nanocomposites, the antibacterial properties of them were compared with the other two different Ag-containing materials (synthesized Ag and Ag_2O NPs) by measuring the viability of bacteria. Ag/MCM-41 NFs, Ag and Ag_2O NPs with the same Ag concentration (26.32 and 12.63 μg/mL for *E. coli* and 6.31 and 26.32 μg/mL for *S. aureus*) were added to the molten LB-agar media and the mixtures were solidified at room temperature. LB-agar plates contained no drugs and MCM-41 NFs used as controls. The suspension of *E. coli* or *S. aureus* was spread into these plates and incubated at 37 °C. After 24 h incubation, the formation of colonies for both strains appeared in plates containing Ag NPs, Ag_2O NPs, and MCM-41 NFs, as well as controls. However, the presence of Ag/MCM-41 NFs in the LB-agar plates could completely inhibit the formation of colonies for both types of bacteria (Fig. 6). Probably, the much-improved effect of the Ag/MCM-41 nanocomposites was because the supporting matrix MCM-41 type nanofibers could protect the Ag NPs from aggregation and enables the continuous release of Ag ions. The highly dispersed of silver in MCM-41 NFs (10.53 wt%) can stably release Ag ions.

The results demonstrated that the Ag/MCM-41 NFs nanocomposites exhibited enhanced antibacterial activity in both *E. coli* and *S. aureus*, and it was closely related to their structure (uniformly distributed Ag NPs), surface

Table. 2: Investigation antibacterial activity.

MCM-41 NFs (Ag or Ag_2O NPs)			500Ag/MCM-41NFs		600Ag/MCM-41NFs	
Bactria	MIC (ppm)	MBC (ppm)	MIC (ppm)	MBC (ppm)	MIC (ppm)	MBC (ppm)
Escherichia coli	Not effective	Not effective	30	60	120	120
Staphylococcus aureus	Not effective	Not effective	60	120	120	250

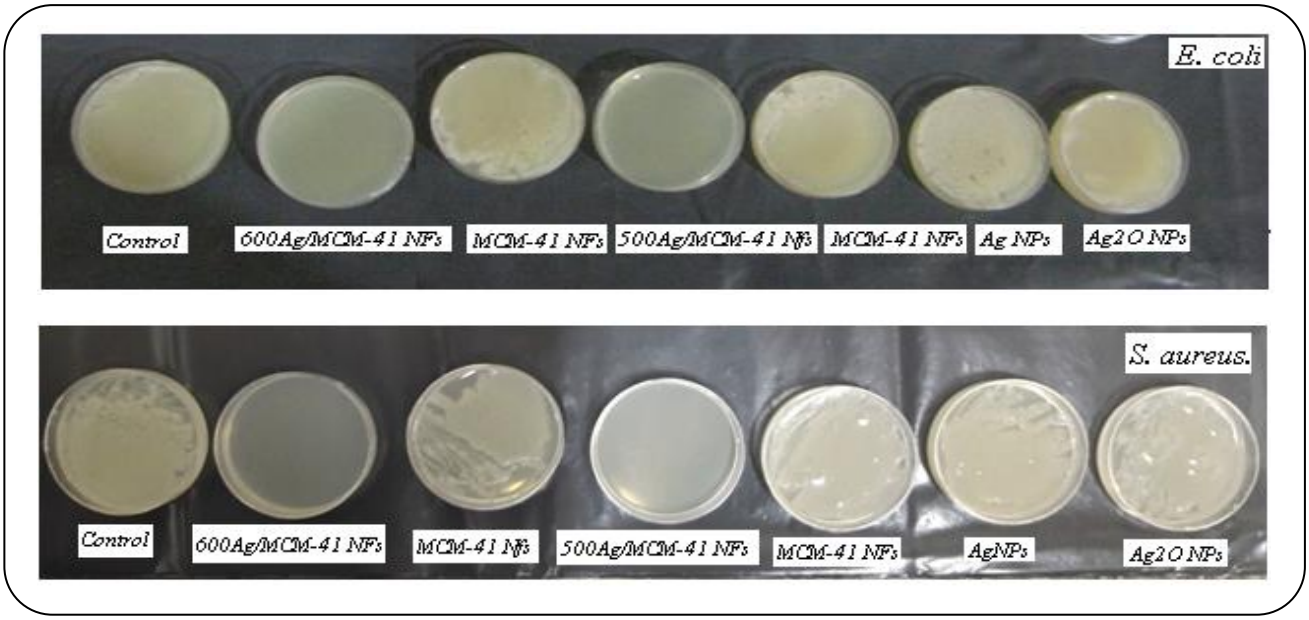

Fig. 6: Antibacterial activities of 600Ag/MCM-41 NFs, MCM-41 NFs, 500Ag/MCM-41 NFs, Ag NPs and Ag_2O NPs samples after incubation with 1 × 10^8 CFU/mL bacteria for 24 h. The number of samples was mentioned for E. coli and S. aureus.

charge (positive charges), and size (10−15 nm). Previous studies have summarized several possible antibacterial mechanisms of Ag NPs [33]. Ag NPs will release Ag^+ ions can interact with thiol groups of vital proteins, which will result in the inactivation of enzyme proteins and disruption of respiration. This is often considered as the main mechanism of the antimicrobial activity of Ag NPs. The release rate of Ag^+ ions depends in part on the size of Ag NPs; the Ag NPs with smaller size might produce faster Ag^+ ion release [34]. In actual application, the complex cultural environment and the dead bacteria often cause the aggregation of Ag NPs, whose larger size decreased the release of Ag^+ ions, leading to a decrease of antibacterial activity. In this study, the Ag NPs loaded in MCM-41 NFs can effectively prevent aggregation and thus retain good disparity in the culture media. The good distribution of Ag NPs makes Ag ions release steadily from nanofibers over a long period and ultimately realize long-term make them adhere to the surface of negatively charged bacteria easily [35]. In most cases, the diameter of Ag NPs in silica materials ranges from 20 to 50 nm [36]; however, in our study, the Ag NPs in MCM-41 NFs carrier were only 10−15 nm, which contributes their increased antibacterial effects. Compared to larger Ag NPs, they may have a faster release of Ag ions, thus inducing higher antibacterial activity.

Compared with 500Ag/MCM-41NFs, the 600Ag/MCM-41NFs sample showed low antibacterial activity. For solid support systems, some researchers have argued that Ag^+ ions released from the surface of metallic silver NPs are responsible for their antibacterial activity [37]. Consistent with the XRD and DRS results, based on analysis of Ag_2O to metallic silver in the 600Ag/MCM-41NFs sample, the content of Ag NPs in the 600Ag/MCM-41NFs sample was more than the 600Ag/MCM-41NFs sample. The results revealed that the Ag NPs in MCM-41NFs matrix indicated low antibacterial activity. Probably, Ag Nps were very stable

in MCM-41NFs matrix and not oxidatively released Ag ions from NPs surface when the 600Ag/MCM-41NFs interacts with an aqueous phase. On the other hand, recent studies have tested the antibacterial effect of different Ag-based materials and showed that their effect is ordered as follows: AgO > Ag_2O > Ag [38] and $AgNO_3$ > Ag-ZSM-5 > Ag_2O > commercial Ag-exchanged zeolite (granular) > commercial Ag-exchanged zeolite (pellets) > Ag nanoparticles (NPs) [39]. Although the antibacterial performance of materials with different Ag valence varies in treating various bacteria, the general consensus is that high valence oxides of Ag, such as AgO, possess a strong bactericidal effect. This can be reasoned for high antibacterial activity in the 500Ag/MCM-41NFs sample concerning 600Ag/MCM-41NFs nanocomposite.

CONCLUSIONS

We describe the synthesis of silver-containing MCM-41 NFs through the heat treatment process. The Ag and Ag_2O NPs with small sizes (10-15 nm) had a high density and well-dispersed distribution in the framework of MCM-41 type nanofibers. The NFs can protect silver compounds from aggregation and allow Ag ions to continuously release from the MCM-41 nanofibers. Thus, Ag/MCM-41 NFs showed long-term antibacterial activity on Gram-negative and Gram-positive bacteria at a low concentration. These NPs have good biocompatibility. In summary, the MCM-41 NFs containing more Ag_2O NPs demonstrated high antibacterial activity concerning Ag/MCM-41 NFs.

Acknowledgments

The authors are thankful for the postgraduate office of Guilan University for the support of this work.

Received : Sep. 30, 2018 ; Accepted : Jan. 28, 2019

REFERENCES

[1] Rai M., Yadav A., Gade A., Silver Nanoparticles as a New Generation of Antimicrobials, *Biotechnol. Adv.*, **27**: 76-83 (2009).

[2] Lalueza p., Monzón M., Arruebo M., Santamaría J., Bactericidal Effects of Different Silver-Containing Materials, *Mater. Res. Bull.*, **46**:2070–2076 (2011).

[3] Liong M., France B., Bradley K.A., Zink J.I., Antimicrobial Activity of Silver Nanocrystals Encapsulated in Mesoporous Silica Nanoparticles, *Adv. Mater.*, **21**:1684–1689 (2009).

[4] Sohrabnezhad Sh., Rassa M., Seifi A., Green Synthesis of Ag Nanoparticles in Montmorillonite, *Mater. Let.*, **168**:28–30 (2016).

[5] Schneider O.D., Loher S., Brunner T.J., Schmidlin P., Stark W.J., Flexible, Silver Containing Nanocomposites for the Repair of Bone Defects: Antimicrobial Effect Against E. Coli Infection and Comparison to Tetracycline Ccontaining Scaffolds, *J. Mater. Chem.*, **18**: 2679–2684 (2008).

[6] Chen Ch-Ch., Wu H-H., Huang H.-Y., Ch.-W Liu., Y.-N Chen., Synthesis of High Valence Silver-Loaded Mesoporous Silica with Strong Antibacterial Properties, *Int. J. Environ. Res. Pub. Health*, **13:** 99-111 (2016).

[7] Aruguete D.M., Kim B., Hochella M.F., Ma Y., Cheng Y., Hoegh A., Liu J., Pruden A Antimicrobial Nanotechnology: Its Potential for the Effective Management of Microbial Drug Resistance and Implications for Research Needs in Microbial Nanotoxicology, *Environ. Sci.: Process. Impacts*, **15**: 93–102 (2013).

[8] Chang Y-H., Lu Y-C., Chou K-S., Enhancement of Photoluminescence of Different Quantum Dots by Ag@SiO_2 Core-Shell Nanoparticles, *Mater. Res. Bull.*, **48**: 2076–2078 (2013).

[9] Wang J-X., Wen L-X., Wang Zh-H., Chen J-F., Immobilization of Silver on Hollow Silica Nanospheres and Nanotubes and Their Antibacterial Effects, *Mater. Chem. Phys.*, **96**: 90–97 (2006).

[10] Kim Y.H., Lee D.K., Cha H.G., Kim C.W., Kang Y.S., Synthesis and Characterization of Antibacterial Ag-SiO_2 Nanocomposite, *J. Phys. Chem.*, **111**: 3629–3635 (2007).

[11] Sohrabnezhad Sh., Sadeghi A., Matrix Effect of Montmorillonite and MCM-41 Matrices on the Antibacterial Activity of Ag_2CO_3 Nanoparticles, *Appl. Clay. Sci.*, **105–106**: 217–224 (2015).

[12] Tian Y., Qi J., Zhang W., Cai Q., Jiang X., Facile, One-Pot Synthesis, and Antibacterial Activity of Mesoporous Silica Nanoparticles Decorated with Well-Dispersed Silver Nanoparticles, *Appl. Mater. Interfaces.*, **6**: 12038−12045 (2014).

[13] Xue X.M., Li F.T., Removal of Cu(II) from Aqueous Solution by Adsorption onto Functionalized SBA-16 Mesoporous Silica, *Microporous Mesoporous. Mater.*, **116**:116–122 (2008).

[14] Kawashita M., Tsuneyama S., Miyaji F., Kokubo T., Kozuka H., Yamamoto K., Antibacterial Silver-Containing Silica Glass Prepared by Sol-Gel Method, *Biomaterials*, **21**: 393-398 (2000).

[15] Jeon H.J., Yi S.C., Oh S.G., Preparation and Antibacterial Effects of Ag-SiO_2 Thin Films by Sol-Gel Method, *Biomaterials*, **24**: 4921-4928 (2003).

[16] Choma J., Jaroniec M., Burakiewicz-Mortka W., Kloske M., Critical Appraisal of Classical Methods for Determination of Mesopore Size Distributions of MCM-41 Materials, *Appl. Surf. Sci.*, **196**: 216-223 (2002).

[17] Lu Q., Gao F., Komarneni S., Mallouk T.E., Ordered SBA-15 Nanorod Arrays Inside a Porous Alumina Membrane, *J. Am. Chem. Soc.*, **126**: 8650-8651 (2004).

[18] Bruinsma P.J., Kim A.Y., Liu J., Baskaran S., Mesoporous Silica Synthesized by Solvent Evaporation: Spun Fibers and Spray-Dried Hollow Spheres, *Chem. Mater.*, **9**: 2507-2512 (1997).

[19] Julian-Lopez B., Boissiere C., Chaneac C., Grosso D., Vasseur S., Miraux S., Duguet E., Sanchez C., Mesoporous Maghemite–Organosilica Microspheres: A Promising Route Towards Multifunctional Platforms for Smart Diagnosis and Therapy, *J. Mater. Chem.*, **17**: 1563-1569 (2007).

[20] Pega S., Boissiere C., Grosso D., Azaıs T., Chaumonnot A., Sanchez C., Direct Aerosol Synthesis of Large-Pore Amorphous Mesostructured Aluminosilicates with Superior Acid-Catalytic Properties, *Angew. Chem. Int. Ed.*, **48**: 2784-2787 (2009).

[21] Balkus Jr K.J., Scott A.S., Gimon-Kinsel M.E., Blanco J.H., Oriented Films of Mesoporous MCM-41 Macroporous Tubules *via* Pulsed Laser Deposition, *Microporous Mesoporous Mater*, **38**: 97-105 (2000).

[22] Cai Q., Luo ZS., Pang W.Q, Fan Y.W., Chen X.H., Cui F.Z., Dilute Solution Routes to Various Controllable Morphologies of MCM-41 Silica with a Basic Medium, *Chem. Mater*, **13**: 258− 263 (2001).

[23] Chen F., Liu Z., Liu Y., Fang P., Dai Y., Enhanced Adsorption and Photocatalytic Degradation of High Concentration Methylene Blue on Ag_2O-Modified TiO_2-Based Nanosheet, *Chem. Eng. J.*, **221**:283-291 (2013).

[24] Dong H., Chen G., Sun J., Li Ch., Yu Y., Chen D., A Novel High-Efficiency Visible-Light Sensitive Ag_2CO_3 Photocatalyst with Universal Photodegradation Performances: Simple synthesis, Reaction Mechanism and First-Principles Study, *Appl. Catal. B*, **134-135**: 46-54 (2013).

[25] Lewis G.N., Concerning Silver Oxide and Silver Suboxide, *J. Am. Chem. Soc.*, **28**: 139-158 (1906).

[26] Jabariyan Sh., Zanjanchi M.A., A Simple and Fast Sonication Procedure to Remove Surfactant Templates from Mesoporous MCM-41. *Ultrason. Sonochem.*, **19**:1087-1093 (2012).

[27] Zhou W., Liu H., Wang J., Liu D., Du G., Cui J., Ag_2O/TiO_2 Nanobelts Heterostructure with Enhanced Ultraviolet and Visible Photocatalytic Activity. *Appl. Mater. Interfaces*, **2**: 2385-2392 (2010).

[28] Xu X., Shen X., Zhou H., Qiu D., Zhu G., Chen K., Facile Microwave-Assisted Synthesis of Monodispersed Ball-Like Ag@ AgBr Photocatalyst with High Activity and Durability, *Appl. Catal.*, **455**: 183-192 (2013).

[29] Xiu Z.M., Zhang Q.B., Puppala H.L., Colvin V.L., Alvarez P.J.J., Negligible Particle-Specific Antibacterial Activity of Silver Nanoparticles. *Nano. Lett.*, **12**: 4271−4275 (2012).

[30] Feng Q.L., Wu J., Chen G.Q., Cui F.Z., Kim T.N., Kim J.O., A Mechanistic Study of the Antibacterial Effect of Silver Ions on Escherichia coli and Staphylococcus Aureus, *J. Biomed. Mater. Res.*, **52**: 662−668 (2000).

[31] Egger S., Lehmann R.P., Height M.J., Loessner M.J., Schuppler M., Antimicrobial Properties of a Novel Silver–Silica Nanocomposite Material, *Appl. Environ. Microbio.*, **75**: 2973–2976 (2009).

[32] Ma Z., Ji H., Tan D., Teng Y., Dong G., Zhou J., Qiu J., Zhang M., Silver Nanoparticles Decorated, Flexible SiO_2 Nanofibers with Long-Term Antibacterial Effect as Reusable Wound Cover. *Colloids Surf. A.*, **387**:57−64 (2011).

[33] Moritz M., Geszke-Moritz M., The Newest Achievements in Synthesis, Immobilization and Practical Applications of Antibacterial Nanoparticles, *Chem. Eng. J.*, **228**: 596–613 (2013).

[34] Zhang W., Yao Y., Sullivan N., Chen Y., Modeling the Primary Size Effects of Citrate-Coated Silver Nanoparticles on Their Ion Release Kinetics. *Environ. Sci. Technol.*, **45**:4422−4428 (2011).

[35] Li L., Wang H., Antibacterial Agents: Enzyme-Coated Mesoporous Silica Nanoparticles as Efficient Antibacterial Agents In Vivo. *Adv. Healthcare Mater.*, **2**:1298−1298 (2013).

[36] Zienkiewicz Strzałka M., Pasieczna Patkowska S., Kozak M., Pikus S., Silver Nanoparticles Incorporated onto Ordered Mesoporous Silica from Tollen's Reagent. *Appl. Surf. Sci.*, **266**: 337−343 (2013).

[37] Pandiyarajan T., Udayabhaskar R., Vignesh S., Arthur James R., Karthikeyan B., Synthesis and Concentration Dependent Antibacterial Activities of CuO Nanoflakes, *Mater. Sci. Eng. C*, **33**:2020–2024 (2013).

[38] Shen W., Feng L., Feng H., Kong Z., Guo M., Ultrafine silver(II) Oxide Particles Decorated Porous Ceramic Composites for Water Treatment, *Chem. Eng. J.*, **175**:592–599 (2011).

[39] Lalueza P., Monzón M., Arruebo M., Santamaría J., Bactericidal Effects of Different Silver-Containing Materials, *Mater. Res. Bull.*, **46**:2070–2076 (2011).